Absence of Dystrophin Related Protein-2 disrupts Cajal bands in a patient with Charcot-Marie-Tooth disease

Accepted Manuscript

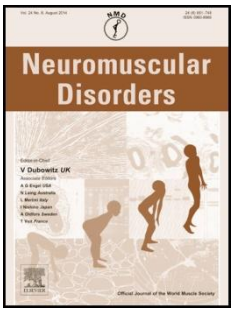

Title: Absence of *Dystrophin Related Protein-2* disrupts Cajal bands in a patient with Charcot-Marie-Tooth disease

Author: Kathryn M. Brennan, Yunhong Bai, Chiara Pisciotta, Suola Wang, Shawna M.E. Feely, Mark Hoegger, Laurie Gutmann, Steven A. Moore, Michael Gonzalez, Diane L. Sherman, Peter J. Brophy, Stephan Züchner, Michael E. Shy

PII: S0960-8966(15)00659-8
DOI: http://dx.doi.org/doi:10.1016/j.nmd.2015.07.001
Reference: NMD 3061

To appear in: *Neuromuscular Disorders*

Received date: 10-3-2015
Revised date: 28-6-2015
Accepted date: 1-7-2015

Please cite this article as: Kathryn M. Brennan, Yunhong Bai, Chiara Pisciotta, Suola Wang, Shawna M.E. Feely, Mark Hoegger, Laurie Gutmann, Steven A. Moore, Michael Gonzalez, Diane L. Sherman, Peter J. Brophy, Stephan Züchner, Michael E. Shy, Absence of *Dystrophin Related Protein-2* disrupts Cajal bands in a patient with Charcot-Marie-Tooth disease, *Neuromuscular Disorders* (2015), http://dx.doi.org/doi:10.1016/j.nmd.2015.07.001.

Title page:

Absence of *Dystrophin Related Protein-2* disrupts Cajal bands in a patient with Charcot-Marie-Tooth disease

Kathryn M. Brennan[1], Yunhong Bai[1], Chiara Pisciotta[1], Suola Wang[1], Shawna M.E. Feely[1], Mark Hoegger[1], Laurie Gutmann[1], Steven A. Moore[2], Michael Gonzalez[3], Diane L. Sherman[4], Peter J. Brophy[4], Stephan Züchner[3], Michael E. Shy[1].

[1] Department of Neurology, University of Iowa, 200 Hawkins Drive, Iowa City, IA 52242, USA

[2] Department of Pathology, Roy J. and Lucille A. Carver College of Medicine, University of Iowa, Iowa City, IA 52242, USA

[3] Department of Human Genetics and Hussmann Institute for Human Genomics, Miller School of Medicine, University of Miami, Miami, FL 33136, USA

[4]Centre for Neuroregeneration, University of Edinburgh, Edinburgh, EH16 4UU, Scotland, UK

Author for correspondence: Kathryn Brennan

Full address for correspondence: 200 Hawkins Drive, Department of Neurology, Carver College of Medicine, University of Iowa Hospitals and Clinics, Iowa City, IA, 52242, USA.

Telephone: 319-353-5076

Fax: 319-384-8476

Email address: katiebre@doctors.org.uk

Highlights:

- We have identified the first CMT patient with a mutation in *DRP2*.
- The mutation, Q269*, is predicted to result in an absence of the protein product.
- Skin biopsy studies confirm this and recapitulate null animal model findings.

Abstract:

Using exome sequencing in an individual with Charcot-Marie-Tooth disease (CMT) we have identified a mutation in the X-linked dystrophin-related protein 2 *(DRP2)* gene. A 60-year-old gentleman presented to our clinic and underwent clinical, electrophysiological and skin biopsy studies. The patient had clinical features of a length dependent sensorimotor neuropathy with an age of onset of 50 years. Neurophysiology revealed prolonged latencies with intermediate conduction velocities but no conduction block or temporal dispersion. A panel of 23 disease causing genes was sequenced and ultimately was uninformative. Whole exome sequencing revealed a stop mutation in *DRP2*, c.805C>T (Q269*). DRP2 interacts with periaxin and dystroglycan to form the periaxin-DRP2-dystroglycan complex which plays a role in the maintenance of the well-characterized Cajal bands of myelinating Schwann cells. Skin biopsies from our patient revealed a lack of DRP2 in myelinated dermal nerves by immunofluorescence. Furthermore electron microscopy failed to identify Cajal bands in the patient's dermal myelinated axons in keeping with ultrastructural pathology seen in the *Drp2* knockout mouse. Both the electrophysiologic and dermal nerve twig pathology support the interpretation that

this patient's *DRP2* mutation causes characteristic morphological abnormalities recapitulating the Drp2 knockout model and potentially represents a novel genetic cause of CMT.

Keywords:

Charcot-Marie-Tooth disease; Hereditary Motor and Sensory Neuropathy; Whole exome sequencing; Nerve conduction studies; Myelin

[1]Abbreviations:

[1] DRP2/drp2= dystrophin-related protein 2; CMT= Charcot-Marie-Tooth disease; PDG= periaxin-DRP2-dystroglycan complex; AD= autosomal dominant; AR=autosomal recessive; NCS= nerve conduction studies; WES= whole exome sequencing; EM= electron microscopy; CSF= cerebrospinal fluid; CIDP= chronic inflammatory demyelinating polyneuropathy; CMTNSv2= Charcot-Marie-Tooth neuropathy score version 2; MLPA=multiplex ligation-dependent probe amplification; *GDAP1* = Ganglioside-induced differentiation-associated protein 1; GEM.app= Genomes Management Application software; NHLBI EVS= National Heart, Lung and Blood Institute Exome Variant Server; PGP= protein gene product 9.5; MBP= myelin basic protein;

1. Introduction:

Dystrophin-related protein 2 (DRP2) is a protein of particular interest to the peripheral nerve as it contributes to the periaxin-DRP2-dystroglycan (PDG) complex at the abaxonal (i.e. outermost or furthest from the axon) myelin membrane that leads to the creation of Cajal bands. Within well-defined geographic domains of myelinating Schwann cell surface membranes, DRP2 interacts with periaxin and dystroglycan to form the PDG complex [1]. The PGD complexes are responsible for linking extracellular matrix proteins such as laminin to myelin (see Figure 2I). This crosslinking occurs via the extracellular α subunit and the transmembrane β subunit of dystroglycan. These complexes are responsible for creating zones of adhesion between the abaxonal surface of compact peripheral nerve myelin and the Schwann cell plasma membrane. Between these zones of adhesion lie the Cajal bands, which are cytoplasm filled channels first described histologically over 100 years ago [2-4].

Autosomal recessive (AR) mutations in periaxin are well described causing a severe demyelinating neuropathy in humans (CMT4F) with onset in infancy and early childhood [5, 6].

BTK= Bruton agammaglobulinemia Tyrosine Kinase; GERP=genomic evolutionary rate profiling; LRT=Likelihood ratio test; SIFT= Sort intolerant from tolerant

Similarly mutations in periaxin have been found to cause a severe demyelinating neuropathy in mice [7, 8]. Despite never being implicated in human disease a *Drp2* null mouse has been generated to investigate the role of the PDG complex further [9]. *Drp2* knockout mice lack Cajal bands and display myelin abnormalities but do not develop weakness or abnormal nerve conductions [9].

Charcot-Marie-Tooth disease (CMT) is the most common inherited neurological condition with a prevalence of around 1:2500 [10]. A heterogeneous disorder, the CMT neuropathies are divided into subtypes by the pattern of inheritance and peripheral nerve conduction studies (NCS). Subtypes include autosomal dominant (AD) demyelinating (CMT 1), AD axonal (CMT 2), AR (CMT 4), X-linked (CMTX) and the more recently described CMT with intermediate NCS (reviewed in [11]. CMT 1 typically has slow nerve conduction velocities (<38m/s in the upper extremities) and pathological evidence of hypertrophic demyelinating neuropathy whereas CMT 2 has relatively normal nerve conduction velocities (NCVs) with evidence of axonal degeneration [12]. CMT Intermediate patients have intermediate NCVs i.e. between 35-45 m/sec in upper extremities. Despite progress in identifying new causal genes in CMT over the last 20 years around 70 % of CMT2 patients remain without a diagnosis [13, 14]. Causal genes in intermediate CMT continue to be described but again the majority remain unknown. Identification of the causal gene is the key step in understanding the pathophysiology of each CMT subtype and a pre-requisite for designing therapeutic strategies.

Whole exome sequencing (WES) has demonstrated ability to identify new causal genes in CMT [15]. Targeted enrichment and resequencing of almost all protein-encoding genes or exons is

undertaken in WES. Whilst exons only represent ~1-2% of the human genome around 85% of Mendelian diseases are caused by mutations in this region [16]. We have used WES to identify a stop mutation in *DRP2* on the X-chromosome. This gene has not previously been shown to cause CMT. We performed immunofluorescence and electron microscopy (EM) studies in skin biopsies from the proband that demonstrate a lack of DRP2 and Cajal bands in peripheral nerve myelin recapitulating the findings reported in the *Drp2* knockout mouse model and supporting the proposition that this *DRP2* stop mutation is a rare cause of CMT.

2. Materials and methods:

2. 1 Consent and exome sequencing

A patient with neuropathy suggestive of CMT was identified along with family members. Informed consent according to the declaration of Helsinki was obtained from all individuals and the Institutional Review Boards at the participating centres approved the study. Neurological examination, neurophysiological and skin biopsy studies were performed on the patient.

2.2 Immunofluorescence:

Skin biopsies for immunofluorescence were obtained using a 2.5mm punch from the lateral aspect of proximal phalanx of the index finger. Biopsies for western blotting and EM studies were also taken in a similar manner from non-glabrous skin on the forearm and upper arm. Skin samples destined for immunofluorescence staining were fixed in 4% paraformaldehyde in PBS (which is diluted from 16% paraformaldehyde solution in ddH_20) for 30 minutes at room temperature. Samples were then washed in PBS three times, and gradually frozen in a

methylbutane container that was placed in a liquid nitrogen small tank and embedded in OCT. Once tissues were hardened (usually 3-5 minutes) they were transferred into a cryostat at -20°C and cut into 20 µm sections (60 µm sections were cut for internodal length assessment). Sections were mounted onto Superfrost glass slides (Fisher Scientific) and stored at -20°C.

Slides were then permeabilized with 100% acetone for 10 minutes, blocked with 5% fish gelatin (Sigma # G7765) for 1 hour. Incubation with primary antibody was overnight at 4°C. After slides were washed in PBS they were incubated with the secondary antibody for 2 hours. A summary of the characteristics and features of each of the primary and secondary antibodies is provided in Supplementary Table 3. Slides were then washed, dried and coverslipped for evaluation using a Leica laser confocal SP5 II microscope. Images were obtained using a 40X objective. All image parameters including pinhole size, detector gain, amplifier offset, amplifier gain and laser intensity were first set for normal control tissue with the same settings used for all samples imaged. All samples images were obtained 24 hours after staining. Slides were stored at -4°C prior to imaging.

Image analysis was performed using Image J software (NIH, Bethseda, MD, USA). Fluorescence intensity was measured for both α-tubulin and the axonal marker, PGP, choosing an intensity threshold in the PGP channel. Then the α-tubulin: PGP ratio was calculated in order to obtain a relative value of α-tubulin intensity with respect to PGP intensity. Similarly we investigated relative intensity of α-tubulin and MBP in this series of experiments. For α/β-dystroglycan and MBP studies we chose an intensity threshold in the MBP channel so that only myelinated axons were highlighted, corresponding to where the PDG complex would normally be found. As

before we calculated the α/β-dystroglycan: MBP ratio to obtain a relative value of α/β-dystroglycan intensity with respect to MBP intensity. For immunofluorescence analysis of the data (which was non-parametric) statistical comparisons were made using unpaired T tests.

2.3 Internodal length:

For the internodal length study LIF files were opened with ImageJ software (NIH, Bethseda, MD, USA).The internodes were identified by morphology using MBP as a myelin marker and PGP as an axonal marker. The length was captured by confocal imaging and measured using Leica Advanced Fluorescence Lite (Leica microsystems Inc, IL, USA) software.

For the supplementary video files confocal images with a Z-series slice thickness of 1µm were processed in automated volume rendering software (Imaris, version 7.6.4, Bitplane) from original LIF (Leica Image File) files. Surfaces were generated based off the fluorescence intensity for a given channel. Individual channels were processed separately and a video was produced by rotating selected rendered channels

2.4 Electron Microscopy:

Skin samples destined for EM were fixed in 2.5% glutaraldehyde in PBS overnight and then subjected to a series of PBS washes (3 in total). Samples were then osmicated in 1% osmium

tetroxide for 1.5 hours. Samples were dehydrated in a series of ethanol dilutions (50, 80, 90 and 100%) propylene oxide, and propylene: epon (50:50) and then embedded in epoxy resin (epon). Tissue blocks were sectioned in 1µm thickness and then stained with toluidine blue for light microscopic examination to locate dermal nerve fascicles. Tissue blocks were then trimmed to cut ultrathin sections, which were then picked up on grids and stained with lead citrate and uranyl acetate for electron microscopy examination. Ultrastructural images were obtained with a digital camera from Advanced Microscopy Techniques on a JEOL JEM-1011 electron microscope.

2.5 Western blotting:

Snap frozen human skin biopsy samples were pulverized, dissolved in lysis buffer (Radioimmunoprecipitation assay buffer (RIPA) buffer, Sigma R0278 and proteinase inhibitors), kept on ice for at least 30 min and centrifuged at 14 000 *g* for 10 min at 4°C. The protein content of the supernatant was determined using a bovine serum albumin standard curve. Equal amounts of the protein were loaded and run on 10% sodium dodecyl sulfate (SDS)–polyacrylamide gel electrophoresis (PAGE) gels, and then transferred onto polyvinyl difluoride membranes. Results were normalized for β-actin (1:20,000) .The primary antibodies used are listed in Supplementary Table 3. Horseradish peroxidase-conjugated secondary antibodies (1:5000–1:20, 000 dilutions; Sigma) were detected using enhanced chemiluminescence (ECL) reagents (Amersham ECL Prime Western Blotting Detection Reagent, RPN 2232) with autoradiography film (Kodak Scientific Imaging Film, Blue XB).

3. Results:

3.1 Clinical findings:

The proband, a 60 year old man, first became symptomatic at age 50 when he noticed a reduction in strength in the lower limbs in addition to poor balance and numbness distally in the lower limbs. He particularly noticed difficulties standing on his toes and that his calves had atrophied in the several years prior to his visit. As an infant he reached all his developmental milestones on time. He reported that he kept up with his peers throughout childhood and adolescence. It was noted however that he always had thin ankles and calves. Clinical examination revealed distal weakness with initial neurophysiologic studies revealing prolonged latencies with conduction velocities in the intermediate range from 36-52m/s (see Table 1). Upper limb amplitudes were normal apart from right sensory ulnar response that was mildly decreased at 16 μV (normal >18). Right sural and superficial peroneal responses were absent. There was no conduction block or temporal dispersion. EMG revealed slight reduction in recruitment in tibialis anterior and first dorsal interosseous. CSF examination at presentation revealed minimally elevated protein. A diagnosis of Chronic Inflammatory Demyelinating Polyneuropathy (CIDP) was made and he was prescribed steroids and three separate courses of intravenous immunoglobulin. Despite this treatment he did not improve and he self-referred to our CMT clinic in 2012 where clinical and neurophysiologic studies were performed with similar results to those performed earlier (see Table 1). Clinical impairment was scored using the validated Charcot-Marie-Tooth neuropathy score (CMTNSv2) and he had a score of 14 indicating a moderate level of disability [17]. Specifically clinical examination revealed slight pes cavus with atrophy of both feet and calves (see Figure 1). The anterior component of both

calves was more significantly atrophied than the posterior component. Both Achilles tendons were tight. He demonstrated mild weakness of tibialis anterior (4+/5), great toe dorsiflexion (4-/5) and great toe plantar flexion (4/5) bilaterally. In the lower limbs there was a demonstrable length dependent reduction in appreciation to pinprick, light touch, vibration (using a Rydell tuning fork) and joint position sense. Pinprick sensation was reduced at toes and ankles. Light touch was absent at toes and reduced at ankles. Vibration was absent at toes and ankles and reduced at the knees. Joint position sense was reduced at the toes only. He had normal reflexes apart from absent ankle jerks bilaterally. Babinski reflexes were absent. His gait was wide based and he was unable to perform tandem gait. He was unable to walk on his toes or heels. Romberg sign was present. In 2013 he developed an episode of lower trunk brachial neuritis characterized by right shoulder girdle pain followed several weeks later by weakness involving the intrinsic muscles of the right hand. These symptoms mostly spontaneously resolved. Despite this resolution he had noticed evolving weakness of both hands by 2014 and reported difficulties buttoning shirts. Clinical examination at this time revealed progression of disease with great toe dorsiflexion now scoring 0/5. Some mild weakness involving the right hand was attributed to the episode of brachial plexopathy. Despite the progression in his symptoms his CMTNSv2 remained 14.

A detailed family history was taken as illustrated in Figure 1. Family member II.5, a maternal second cousin, who was not examined in our clinic, has a diagnosis of peripheral neuropathy. The index case provided us with her history. The relative first presented in her late 50s with

distal ankle weakness with a history of high arches, hammer toes and requires ankle foot orthotic devices to ambulate.

3.2 Genetic testing and genomic studies

Due to the lack of response to immunoglobulin the possibility of a genetic neuropathy was raised and genetic testing was undertaken at Athena Diagnostics. A comprehensive panel of 23 CMT disease causing genes was sequenced with MLPA analysis performed on 2 genes (*PMP-22* and *GJβ1*) (Supplementary Table 1). This testing was uninformative apart from revealing a variant of unknown significance involving *GDAP1* (Ganglioside-induced differentiation-associated protein 1). Located in the Glutathione-S-Transferase domain this variant was not predicted to change the amino acid sequence or have any effect on splicing. Whole exome sequencing was then performed. Using GEM.app [18] software we focused our genomic analysis on rare and conserved variants that followed autosomal dominant, autosomal recessive and X-linked inheritance in whole exome sequencing data. This revealed a stop mutation in the proband, c805 C>T or Q269X, in exon 5 of the *DRP2*. Only variants that met the following criteria were considered to be pathogenic: (i) non-synonymous changes; (ii) not present in NHLB1 EVS 6500; (iii) not present in families within the 2700 families in GEM.app database or in 6500 NHLBI Exome Sequencing project; (iv) Genomic Evolutionary Rate Profiling >3 or PhastCons >0.6 (see Table 2) [19] . Sanger sequencing was performed on unaffected family member III.4. The *DRP2* stop mutation was not identified.

3.3 Immunostaining

3.3.1 DRP2

Immunofluorescence studies revealed a lack of DRP2 staining in all myelinated nerves obtained from the skin biopsies of our patient whereas in healthy controls we consistently observed a patchy pattern of DRP2 immunofluorescence which appears to overly the myelin sheath (see Figure 2A-F and Supplementary Videos 1- 4). We tested for the presence of DRP2 using two specific DRP2 antibodies; 2222, directed against an exon 4 peptide and 2164, which is directed against the C terminus [1, 9]. Neither antibody demonstrated immunoreactivity to DRP2 in the patient's dermal myelinated nerves whereas in all 3 healthy controls the presence of DRP2 on myelinated nerves was easily demonstrable (see Figure 2 and Supplementary Table 2).

3.3.2 Internodal length

A reduction in internodal length has been reported in periaxin deficient mice in addition to reduced conduction velocities [7]. In contrast the *Drp2* deficient mouse had a much more benign phenotype with normal internodal lengths and conduction velocities [9]. We postulated that the internodal lengths of the myelinated nerves in our patient should be unaffected. We only isolated 8 internodes in our patient but despite the small numbers the data was comparable to that previously reported in healthy controls. The mean internodal lengths in our patient with *DRP2* mutation was 89.52 ± SD 14.39µm which is similar to that reported in healthy controls by Saporta et al [20] (94.5 ± SD 28.6 µm).

3.3.3 Tubulin staining

As yet the function of Cajal bands has not been determined. It was originally proposed that they might serve a nutritive purpose and it has been suggested that Cajal bands contain microtubules that serve such a function [7]. In an effort to investigate the microtubule network of transport in myelin we performed immunofluorescence studies investigating tubulin staining using protein gene product 9.5 (PGP) as an axonal marker and myelin basic protein (MBP) as a myelin marker (Supplementary Figure 1). There was no discernible difference in α-tubulin staining in our patient compared to controls suggesting that the microtubule network was still present despite the lack of Cajal bands (p=NS using unpaired T test).

3.3.4 α-dystroglycan and β-dystroglycan staining

Both α-dystroglycan and β-dystroglycan are integral components of the PDG complex (see Figure 2I). We next investigated if staining of these two proteins was abnormal in our patient. There was no difference in α-dystroglycan and β-dystroglycan staining (relative intensity to MBP) in myelinated nerves from the patient compared to controls using unpaired T tests (see Supplementary Figure 2).

3.4 Electron microscopy

We investigated the architecture of these dermal nerves using electron microscopy. No distinct abaxonal appositions were observed in the patient, with most myelinated axons demonstrating a circumferential band of Schwann cell cytoplasm surrounding the abaxonal myelin (Figure 2H). In contrast, abaxonal appositions were readily identified in healthy control dermal nerves (Figure 2G).

4. Discussion:

DRP2 is a small protein which resembles a short C-terminal isoform of dystrophin and dystrophin related protein 1 (or utrophin) [21]. This 879aa protein is encoded by a 45kb gene localized to Xq22 and was originally described as being expressed principally in the brain and spinal cord [21]. Deletions spanning *DRP2* alongside other X-linked genes such as *BTK* have been reported with agammaglobulinaemia and Mohr–Tranebjaerg syndrome [22-24]. More recently, DRP2 truncating mutations have been proposed as a potential cause of autism spectrum disorder though the mechanism remains to be elucidated [25]. While no mutations have been previously described in *DRP2* in CMT, alongside periaxin, DRP2 is an integral component of the PDG complex in myelinating Schwann cells of the peripheral nervous system. As aforementioned the zones of adhesion created by successive PDG complexes in the abaxonal membrane of Schwann cells leads to the development of fluid filled Cajal bands. Although the exact role of Cajal bands remains to be determined it has been suggested from observations in periaxin and *Drp2* knockout models, that the primary role of the PDG complex in these appositions is to stabilize and limit the radial growth of myelin [8, 9].

Immunofluorescence staining of dissected nerves from the *Drp2* knockout animals reveals a complete absence of DRP2. Western blotting confirmed the absence of this protein. Our proband demonstrates a similar paucity of DRP2 immunostaining staining using the same antibodies as described previously (see Figure 2)[9]. We did attempt to confirm the absence of DRP2 with western blotting techniques however no DRP2 was detected in healthy controls, likely due to the minute amount of peripheral nerve in the dermal samples. Our patient's

c.805C>T stop mutation in exon 5 of the *DRP2* gene would be predicted to cause non-sense mediated decay of mRNA or rapid degradation of any truncated protein produced [26] and is consistent with our immunostaining results.

Although we are confident that the stop mutation in *DRP2* is directly responsible for the morphological changes observed in our patients' dermal nerves, we have not established proof that the mutation is directly responsible for the neuropathy. It will therefore be of vital importance to identify and evaluate other patients with *DRP2* stop/null mutations to confirm our hypothesis of causality. Interestingly the relatively benign phenotype of the *Drp2* null mouse is consistent with the late onset of neuropathy in our patient. At 3 weeks the *Drp2* null mice had normal internodal lengths, conduction velocities and motor behaviour. Apparent at this stage however was the loss of abaxonal appositions as seen in our patient (Figure 2). By 6 months the null mice do display abnormalities such as myelin outfoldings, focal hypermyelination, onion bulbs with thin myelin and supernumery Schwann cells but these abnormalities comprise only ~6% total nerve fibres suggesting any clinical neuropathy associated with such a null mutation would be either mild, delayed in onset or both. Interestingly our patient had a disease onset in his 6th decade. An important clinical point is that based on his adult onset, slow nerve conductions and lack of a clear family history he was treated as if this were an acquired demyelinating neuropathy with immunomodulatory treatments. These were ineffective, consistent with our assumption that this is a genetic neuropathy. Based on the neurophysiology we believe this man to have an intermediate form of CMT.

It is noteworthy that skin biopsies can aid in the diagnosis and evaluation of inherited neuropathy. A skin biopsy may to be useful in distinguishing inherited from acquired demyelinating neuropathies by revealing characteristic pathological and molecular architectural changes [20]. For example the internodal length of dermal myelinated nerve fibres is typically uniformly shortened in CMT1A patients compared with healthy controls. Whereas segmental demyelination, a hallmark of chronic inflammatory demyelinating polyneuropathy, is absent in the dermal myelinated nerve fibres of CMT1A patients [20]. More recently our group has observed a reduction in neurofilament expression in dermal nerve fibres in patients with CMT2E that is caused by mutations in the neurofilament light chain gene [27]. Once again skin biopsy has proven useful in the evaluation of inherited neuropathy.

Acknowledgements:

This study was supported by the Inherited Neuropathy Consortium-Rare Disease Clinical Research Consortium (INC-RDCRC-U54NSO65712), National Institute of Neurological Disorders and Stroke/ Office of Rare Diseases Research (NINDS/ORDR), Initiative of National Center for Advancing Translational Sciences (NCATS), the Muscular Dystrophy Association (MDA) and the Charcot-Marie-Tooth Association (CMTA). Steven A. Moore reports National Institutes of Health (NIH) funding for Wellstone Muscular Dystrophy Cooperative Research Center (U54NS053672). Peter J. Brophy acknowledges support from the Wellcome Trust.

References:

[1] Sherman DL, Fabrizi C, Gillespie CS, Brophy PJ. Specific disruption of a schwann cell dystrophin-related protein complex in a demyelinating neuropathy. Neuron 2001;30:677-87.

[2] Nageotte J. Les étranglements de Ranvier et les espaces interannulaires des fibres nerveuses a myéline. Comptes Rendus de l'Association des Anatomistes 1910:15.

[3] Nemiloff A. Über die Beziehung der sog. "Zellen der Schwannschen Scheide" zum Myelin in den Nervenfasen von Säugetieren. Archiv für Mikroskopische Anatomie und Entwicklungsgeschichte 1910:19.

[4] Ramón y Cajal S. El aparato endocelular de Golgi de la célula de Schwann y algunas observaciones sobre la estructura de los tubos nerviosos. Trabajos del Laboratorio de Investigaciones Biológicas de la Universidad de Madrid 1912;10:26.

[5] Guilbot A, Williams A, Ravise N, et al. A mutation in periaxin is responsible for CMT4F, an autosomal recessive form of Charcot-Marie-Tooth disease. Human molecular genetics 2001;10:415.

[6] Marchesi C, Milani M, Morbin M, et al. Four novel cases of periaxin-related neuropathy and review of the literature. Neurology 2010;75:1830.

[7] Court FA, Sherman DL, Pratt T, et al. Restricted growth of Schwann cells lacking Cajal bands slows conduction in myelinated nerves. Nature 2004;431:191-5.

[8] Gillespie CS, Sherman DL, Fleetwood-Walker SM, et al. Peripheral demyelination and neuropathic pain behavior in periaxin-deficient mice. Neuron 2000;26:523-31.

[9] Sherman DL, Wu LM, Grove M, Gillespie CS, Brophy PJ. Drp2 and periaxin form Cajal bands with dystroglycan but have distinct roles in Schwann cell growth. Journal of Neuroscience 2012;32:9419-28.

[10] Skre H. Genetic and clinical aspects of Charcot-Marie-Tooth's disease. Clinical genetics 1974;6:98-118.

[11] Saporta MA, Shy ME. Inherited Peripheral Neuropathies. Neurologic clinics 2013;31:597-620.

[12] Harding AE, Thomas PK. The clinical features of hereditary motor and sensory neuropathy types I and II. Brain 1980;103:259.

[13] Saporta AS, Sottile SL, Miller LJ, Feely SM, Siskind CE, Shy ME. Charcot-Marie-Tooth disease subtypes and genetic testing strategies. Annals of neurology 2011;69:22-33.

[14] Murphy SM, Laura M, Fawcett K, et al. Charcot-Marie-Tooth disease: frequency of genetic subtypes and guidelines for genetic testing. Journal of neurology, neurosurgery, and psychiatry 2012;83:706-10.

[15] Montenegro G, Powell E, Huang J, et al. Exome sequencing allows for rapid gene identification in a Charcot-Marie-Tooth family. Annals of neurology 2011;69:464-70.

[16] Botstein D, Risch N. Discovering genotypes underlying human phenotypes: past successes for mendelian disease, future approaches for complex disease. Nature Genetics 2003;33 Suppl:228-37.

[17] Murphy SM, Herrmann DN, McDermott MP, et al. Reliability of the CMT neuropathy score (second version) in Charcot-Marie-Tooth disease. Journal of the Peripheral Nervous System 2011;16:191.

[18] Gonzalez MA, Lebrigio RF, Van Booven D, et al. GEnomes Management Application (GEM.app): a new software tool for large-scale collaborative genome analysis. Human Mutation 2013;34:842-6.

[19] Montenegro G, Powell E, Huang J, et al. Exome Sequencing Allows for Rapid Gene Identification in a Charcot-Marie-Tooth Disease Family. Journal of the Peripheral Nervous System 2010;515:292.

[20] Saporta MA, Katona I, Lewis RA, Masse S, Shy ME, Li J. Shortened internodal length of dermal myelinated nerve fibres in Charcot-Marie-Tooth disease type 1A. Brain 2009;132:3263.

[21] Roberts RG, Freeman TC, Kendall E, et al. Characterization of DRP2, a novel human dystrophin homologue. Nat Genet 1996;13:223-226.

[22] Sediva A, Smith CI, Asplund AC, et al. Contiguous X-chromosome deletion syndrome encompassing the BTK, TIMM8A, TAF7L, and DRP2 genes. J Clin Immunol 2007;27:640-6.

[23] Jyonouchi H, Geng L, Toruner GA, Vinekar K, Feng D, Fitzgerald-Bocarsly P. Monozygous twins with a microdeletion syndrome involving BTK, DDP1, and two other genes; evidence of intact dendritic cell development and TLR responses. European journal of pediatrics 2008;167:317-21.

[24] Arai T, Zhao M, Kanegane H, et al. Genetic analysis of contiguous X-chromosome deletion syndrome encompassing the BTK and TIMM8A genes. J Hum Genet 2011;56:577-82.

[25] Toma C, Torrico B, Hervas A, et al. Exome sequencing in multiplex autism families suggests a major role for heterozygous truncating mutations. Mol Psychiatry 2014;19:784-90.

[26] Inoue K, Khajavi M, Ohyama T, et al. Molecular mechanism for distinct neurological phenotypes conveyed by allelic truncating mutations. Nature genetics 2004;36:361-9. Epub 2004 Mar 7.

[27] Pisciotta C, Bai Y, Brennan KM, et al. Reduced neurofilament expression in cutaneous nerve fibers of patients with CMT2E. Neurology 2015.

Figure 1: Clinical features and family pedigree

A. Wasting of anterior shin in the proband

B. Wasting of calf muscles in the proband

C. Pedigree structure for the reported patient with *DRP2* mutation. The proband is indicated by the arrow. Individual generations are numbered with Roman numerals on the left. Open symbols represent unaffected individuals. Filled circles = CMT females. Filled squares= CMT males *= individual with *DRP2* stop mutation. Semi-circles= females with hammertoes. Semi-squares=hammertoes. Individual I.3 had an abnormal gait in addition to hammertoes. Individual II.5 has a diagnosis of peripheral neuropathy.

Figure 2: Dermal nerve fibres of the proband lack DRP2

Immunofluorescence staining and electron microscopy of the patient and healthy controls. Panels A-F show immunofluorescent images from a healthy control (A-C) and the patient (D-F) illustrating neurofilament staining the axon in green, myelin basic protein revealing the overlying myelin sheath in blue and DRP2 located at the abaxonal surface of the myelin sheath in red. No discernible DRP2 expression was demonstrated in our patient. G & H, electron

micrographs of transverse sections of dermal axons in control (G) and patient (F). Cajal bands were easily demonstrated in the control patient and are marked with asterisks in red. No distinct Cajal bands were observed in the patient with most myelinated axons demonstrating a circumferential band of Schwann cell cytoplasm surrounding the abaxonal myelin. In addition axonal inclusions are visible in the patient. I= representative diagram of a myelinated axon and the periaxin-DRP2-dystroglycan (PDG) complex.

Table 1: Sequential neurophysiological findings

Date	Nerve	Latency (ms)	Amplitude	Conduction velocity (m/s)
2010	R ulnar motor (wrist)	3.7 (<3.4)	13.4mV (>2.8 mV)	45 (>49)
	R ulnar motor (above elbow)	10.9 (<9.6)	12.2mV (>2.8 mV)	44 (>50)
	R ulnar motor (axilla)	13 (<11.7)	12.0Mv (>2.8 mV)	36 (>53)
	R CP motor	NR	-	-
	R tibial motor	7.3 (<6.0)	2 µV (>2.9mV)	-
	R ulnar sensory	3.8 (<3.1)	16 µV (>18µV)	37 (>44)
	R sural	NR	-	-
2012	L ulnar motor (wrist)	3.7 (<3.4)	10mV (>2.8 mV)	45 (>49)
	L ulnar motor (above elbow)	11.6 (<9.6)	9.2mV (>2.8mV)	42 (>50)
	L ulnar motor (axilla)	13.9 (<11.7)	9.5mV (>2.8mV)	35 (>53)
	R ulnar sensory	3.5 (<3.1)	29 µV (>18 µV)	34 (>44)
	R sural	2.5	6 µV (>10 µV)	48 (39)
2014	R ulnar motor	3.4 (3.4)	8.2mV (>2.8 mV)	43 (>49)

R median motor	4.4 (<4.2)	5.9mV (>3.5 mV)	-
R ulnar sensory	3.2 (<3.1)	18.1 μV (>18 μV)	42 (>44)
R median sensory	3.6 (<3.5)	16.6 μV (>20 μV)	44 (>44)
R median F wave	37.6ms (<29.2ms)		
R ulnar F wave	37.4ms (<29.2ms)		

CP= common peroneal; NR= not recordable

Table 2: *In silico* scores

Severity Prediction	**Value**	**Range**
GERP score	5.46	-12.3 to 6.17
PhastCons	1.00	0 to 1
Mutation Taster	Disease causing	Polymorphism to disease causing
LRT	Deleterious	Unknown, neutral, deleterious
SIFT	Damaging	Tolerated to damaging

GERP=genomic evolutionary rate profiling; LRT=Likelihood ratio test; SIFT= Sort intolerant from tolerant